Dynamics of long-term continuous culture of Limnospira indica in an air-lift photobioreactor

David Garcia-Gragera, Enrique Peiro, Carolina Arnau, Jean-François Cornet, Claude-Gilles Dussap, Francesc Godia

microbial biotechnology

Open Access

Dynamics of long-term continuous culture of *Limnospira indica* in an air-lift photobioreactor

David Garcia-Gragera[1] Enrique Peiro,[1,2] Carolina Arnau,[1,2] Jean-François Cornet,[3] Claude-Gilles Dussap[3] and Francesc Godia[1,2]

[1]*MELiSSA Pilot Plant – Claude Chipaux Laboratory, Universitat Autònoma de Barcelona, Bellaterra, Barcelona, Spain.*

[2]*CERES, Instituts d'Estudis Espacials de Catalunya, Campus UAB, Barcelona, Spain.*

[3]*CNRS, SIGMA Clermont, Institut Pascal, Université Clermont Auvergne, Clermont-Ferrand, France.*

Summary

MELiSSA (Microecological Life Support System Alternative) is a developing technology for regenerative life support to enable long-term human missions in Space and has developed a demonstration Pilot Plant. One of the components of the MELiSSA Pilot Plant system is an 83L external loop air-lift photobioreactor (PBR) where *Limnospira indica* (previously named Arthrospira sp. PC8005) is axenically cultivated in a continuous operation mode for long-periods. Its mission is to provide O_2 and consume CO_2 while producing edible material. Biological and process characterization of this PBR is performed by analysing the effect of two main variables, dilution rate (*D*) and PFD (Photon Flux Density) illumination. A maximum oxygen productivity (r_{O_2}) of 1.35 mmol l^{-1} h^{-1} is obtained at a *D* of 0.025 h^{-1} and PFD of 930 μmol m^{-2} s^{-1}. Photoinhibition can occur when a 1 g l^{-1} cell density culture is exposed to PFD higher than 1700 μmol m^{-2} s^{-1}. This process is reversible if the illumination is returned to dim light (150 μmol m^{-2} s^{-1}), proving the cell adaptability and capacity to respond at different illumination conditions. Influence of light intensity in cell composition is also described. Specific photon flux density (qPFD) has a direct effect on phycobiliproteins and chlorophyll content causing a decrease of 62.5% and 47.8%, respectively, when qPFD increases from 6.1 to 19.2 μmol g^{-1} s^{-1}. The same trend is observed for proteins and the opposite for carbohydrate content. Morphological and spiral structural features of *L. indica* are studied by confocal microscopy, and size distribution parameters are quantified. A direct effect between trichome *width* and CDW/OD ratio is observed. Changes in size distribution are not correlated with environmental factors, further confirms the adaptation capacity of the cells. The systematic analysis performed provides valuable insights to understand the key performance criteria of continuous culture in air-lift PBRs.

Introduction

For decades, projects envisioning sustained human exploration of Space have focused the interest of researchers and space agencies. Feasibility of long-term human exploration missions, including permanent human bases on Mars or the Moon will require advances in several enabling technologies to guarantee their feasibility and safety, including ECLSS (Environmental Control and Life Support System). Among them, bioregenerative life support systems and technologies are called to increase self-sustainability in Space by substantially reducing the needs from regular food supply from Earth. In this context, MELiSSA (Microecological Life Support System Alternative) was conceived as a bioregenerative ECLSS (Mergeay *et al.*, 1988; Lasseur *et al.*, 2010). It is inspired in a terrestrial ecological system, reproducing its main functions in separated microbiological compartments (Hendrickx *et al.*, 2006). A total of six distinct compartments are considered in the MELiSSA loop (Gòdia *et al.*, 2004), with the aim to provide the main functions of food supply, atmosphere revitalization, water reclamation and waste recycling. All of them are operated in continuous mode under controlled conditions and connected to each other through the corresponding gas, liquid and solid interfaces. The overall approach is based on the use of defined microbial cultures in each compartment and the generation of knowledge-based mathematical models supporting the design, monitoring and control of each one of the individual compartments of the loop and the complete system.

Received 25 October, 2020; revised 31 May, 2021; accepted 14 June, 2021.
For correspondence. E-mail david.garcia.gragera@uab.cat; Tel. +34 935 868 172.
Microbial Biotechnology (2021) **0**(0), 1–18
doi:10.1111/1751-7915.13882
Funding information
The MELiSSA Pilot Plant is funded from ESA contributions from Spain (main contributor), Begium, France, Italy and Norway, under Frame Contract C4000109802/13/NL/CP. Co-funding from Ministerio de Ciencia e Innovación (RD 788/2020), Generalitat de Catalunya and Universitat Autònoma de Barcelona is also acknowledged.

Long-term continuous ground demonstration is mandatory in any ECLSS previous to space adaptation and adoption, in order to demonstrate its feasibility, efficiency, reliability and robustness. The MELiSSA Pilot Plant is a facility conceived to provide such integration and demonstration. Its scenario is to produce the oxygen needs of one human and 20%–40% of the food. A key element is to find the optimum performance conditions of each biological compartment to reach the production targets.

The work presented hereafter focuses on the process and biological characterization of one of the compartments in the loop: the photosynthetic bioreactor (C4a in the MELiSSA loop). Even that the motivation of this work arises in the context of the development of the Life Support System MELiSSA focussed on human Space exploration, the results from it should also be of interest and applicability in a much more general context of the use of photobioreactors (PBRs) in advanced bioprocesses based on photosynthetic microorganisms for the production of added value chemicals, food components, waste treatment and biofuels, among others Cultivation of the cyanobacteria *Limnospira indica* (previously known as Arthrospira sp. PC8005) takes place in an external loop air-lift PBR in a continuous operation mode. One main advantage of this type of bioreactor lays on avoiding shear stress on cyanobacterial cells. Mixing is provided by differences of density between the riser, where the gas is sparged, and the downcomer. It creates a circular flow circulation pattern in which the cells flow alternatively through illuminated and non-illuminated zones of the bioreactor (Vernerey *et al*., 2001; Barbosa *et al*., 2003; Gupta *et al*., 2015). They are also interesting because of their high mass transfer rate between gas and liquid phases, avoiding accumulation of O_2 and enabling an efficient CO_2 transfer (Miron *et al*., 2000). The function of the air-lift PBR in the loop is to provide oxygen and edible material. Indeed, *L. indica* was selected because it is edible and has a high protein contents. In the loop, the function of this compartment is complemented by a higher plant chamber. Also as part of the loop, the nitrification compartment provides the necessary Nitrogen source for the growth of cyanobacteria (Clauwaert *et al*., 2017).

Limnospira culture characterization and photosynthesis capacity has received substantial research interest, although most of the work has been performed at Erlenmeyer flasks or lab-scale and in batch experiments. Here, continuous operation of 83 L pilot scale bioreactor is performed during long duration experiments. In such a context, there is a need for a deep understanding of the dynamics of the PBR operation when the culture is exposed to changes in operational conditions. Particularly, it is essential to characterize the biological response of the culture when exposed to light and dilution rate variations. Indeed, these are the two main controlled variables in the MELiSSA loop that are adjusted by its predictive control system to achieve the desired performance in terms of air revitalization and biomass production (Poughon *et al*., 2009).

Extensive previous work has been done on the analysis of the response of cyanobacteria when exposed to high PFD (Photon Flux Density; Vonshak *et al*., 1996; Tomaselli *et al*., 1997), also considering gene expression level (Hihara *et al*., 2001; Muramatsu and Hihara, 2012). It was identified as a potential limitation to reach high productivities in open ponds systems since the very beginning (Vonshak *et al*., 1988; Richmond *et al*., 1990). Optimization of cultivation conditions for high pigment productivities has also been reported (Rodríguez *et al*., 1991; Begum *et al*., 2016). Light availability is often considered as only depending on light intensity, and the relevance of the interaction with cell density has received less attention.

This study aims to investigate the dynamics of *L. indica* cultures under different illumination conditions as well as the influence of long-term operation. Understanding of these dynamics is a fundamental aspect in the MELiSSA loop since inputs variables of each compartment must be continuously adjusted to fit the needs of the crew. An innovative approach regarding treatment of light availability is presented: qPFD (specific PFD), defined in order to assess the influence of both light intensity and cell density on light availability and consequently, in culture performance. This variable is considered of significant relevance in continuous operation of PBR because light availability becomes an output of the liquid flow and light PFD provided by the illumination system. Further, the effect of qPFD on different biomass composition parameters should also be considered. In continuous cultures operating at steady-state, the impact of the previous culture conditions on a given operation condition should also be considered. Indeed, multiplicity of steady sates has been observed in mammalian or bacterial cultures, wherein different cells and product concentration can be reached with the same operational conditions depending on the conditions of the previous steady-state (Follstad *et al*., 1999; Yongky *et al*., 2015). This phenomenon is observed in this work, to the best of our knowledge, for the first time in *L. indica* and is highly related to qPFD value. Additionally, variations in cell size and morphology have been reported in the literature to be an indicator of cell response to fluctuations in environmental conditions (Kaggwa *et al*., 2013), specially related to stress. However, morphology changes observed in this study are not correlated with experimental conditions. These changes are analysed as well as their consequences on online monitoring techniques of PBRs.

Finally, the operational robustness of the PBR is a relevant aspect for long-term operation in a bioregenerative life support systems context, not only in a wide operational range, but also when exposed to extreme light availability situations and its recovery capacity from potential photoinhibition. Indeed, in the scope of the MELiSSA loop, a high PFD scenario could occur if a peak in O_2 demand occurs. In this case, the control system would increase the light up to its maximum to mitigate the lack of O_2, The systematic analysis performed in this work provides valuable insights to understand the key performance criteria of continuous culture in air-lift PBRs.

Results

Process performance under different light and dilution rate conditions

The key operational variables influencing the performance of a PBR are the dilution rate (D) and light intensity (PFD), especially considering that the objective of its operation in the context of MELiSSA is the production of O_2 and consumption of CO_2 for atmosphere revitalization and the production of edible biomass. A total of eight conditions combining different values for D and PFD were tested. One condition ($D = 0.025\ h^{-1}$; PFD = 932 μmol m^{-2} s^{-1}) was tested four times at different time points to analyse the reproducibility of results. The summary of the tested conditions is provided in Table 1. Between Runs 7 and 8 additional conditions were tested as a response to the photoinhibition event further discussed. Figure 1 provides the results of O_2 production and cell density at steady state and during transitory phases for each condition, in a continuous operation of the PBR for a period of 180 days. Steady state is reached in all conditions presented in Fig. 1A. Contrarily, for the last period of Fig. 1B (days 137–171), a photoinhibition effect is observed after setting $D = 0.025\ h^{-1}$ and PFD = 1700 μmol m^{-2} s^{-1} (Run 7b) and consequently steady state is not reached. This last period also includes *Transition phase* ($D = 0.025\ h^{-1}$; PFD = 387 μmol m^{-2} s^{-1}; days 151–164) and *Recovery* ($D = 0\ h^{-1}$; PFD = 150 μmol m^{-2} s^{-1}; days 164–171). Values of oxygen and biomass productivities at steady state are presented in Table 2, which also includes the range of values obtained in Run 7b. The highest oxygen production is obtained with a PFD of 932 μmol m^{-2} s^{-1} and a D of 0.025 h^{-1}. Average production of 3.2 g h^{-1} and an average productivity of $r_{O_2} = 1.19$ mmol l^{-1} h^{-1} are obtained, considering the four repeated conditions. Maximum biomass productivity is also obtained under these conditions because of high dilution rates (r_x = 23.7 mg $X{\cdot}l^{-1}$ h^{-1}), although at a lower biomass concentration at steady state ($X = 0.95$ g l^{-1}). The highest cell concentration ($X = 1.65$ g l^{-1}) is reached in Run 5 (D of 0.01 h^{-1}; PFD of 932 μmol m^{-2} s^{-1}), but this high value penalises O_2 production because of the shadow effect generated by higher cell density. Lowest oxygen productivities are obtained for Runs 2 ($D = 0.014\ h^{-1}$; PFD = 387 μmol m^{-2} s^{-1}) and 3 ($D = 0.025\ h^{-1}$; PFD = 163 μmol m^{-2} s^{-1}) with $r_{O_2} = 0.73$ mmol l^{-1} h^{-1} and $r_{O_2} = 0.4$ mmol l^{-1} h^{-1} respectively. Such low productivities are explained by the lowest PFD. Run 3 also coincides with the lowest cell density (0.32 g l^{-1}). In contrast, Run 2 reaches a cell density of 1 g l^{-1} even at relatively low PFD because of lower dilution rate ($D = 0.014\ h^{-1}$).

Repetition of condition at 932 μmol m^{-2} s^{-1} and 0.025 h^{-1} aims to understand if the conditions in one given steady-state are affected by the conditions experienced by the culture in the previous period. For this, the same condition is repeated four times, but with different conditions in the previous culture step. One-way ANOVA analysis of results for the repeated condition (Runs 1, 4, 6 and 8) indicates that O_2 production mean values are significantly different ($P < 0.05$). The same effect is observed on biomass concentration ($P < 0.05$). O_2 production for Run 4 is 13.6% lower than Run 1, followed by 7% reduction in Run 6. Finally, a recovery is observed in Run 8 where O_2 production increases by 15% compared with Run 6. A new term is included in the results, which is the specific PFD (qPFD). It is defined as the amount of photons provided to the culture per mass of cells. Influence of past qPFD (μmol g^{-1} s^{-1}) on the r_{O_2} of a certain condition is analysed. Pearson's correlation shows that past qPFD has an effect on present r_{O_2} ($r = -0.971$; $P < 0.05$).

Table 1. Summary of tested conditions including values of manipulated variables and starting and final culture day.

Run	PFD (μmol m^{-2} s^{-1})	D (h^{-1})	Starting day	Final day
1	932	0.025	10	22
2	387	0.014	22	40
3	163	0.025	40	50
4	932	0.025	50	62
5	932	0.010	62	88
6	932	0.025	88	99
7	1472	0.014	99	137
7b	1700	0.025	137	151
Transition	387	0.025	151	164
Recovery	150 → 300	0	164	171
8	932	0.025	171	177

Reversibility of photoinhibition effect

The results presented in last period of Fig. 1B correspond to a 30 days period where a photoinhibition phenomenon is observed. On day 137, PFD is increased to

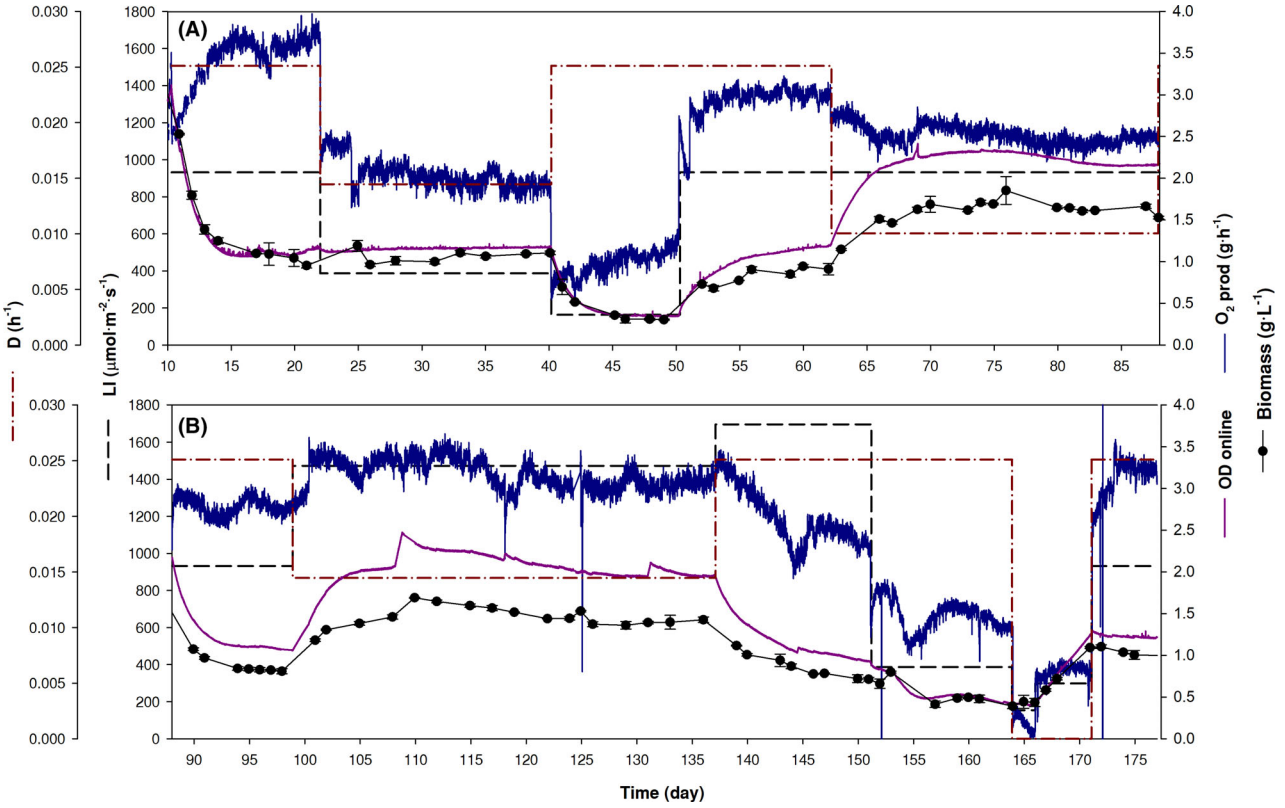

Fig. 1. Evolution of O_2 production (g $\cdot l^{-1}$), online biomass absorbance and cell density (g $\cdot l^{-1}$) during the continuous cultivation carried out at different dilution rates (*D*) and illumination levels (PFD).
A. Depicts results of Run 1 (0.025 h^{-1}; PFD = 932 µmol $\cdot m^{-2}$ $\cdot s^{-1}$), Run 2 (0.014 h^{-1}; PFD = 387 µmol$\cdot$ m^{-2} $\cdot s^{-1}$), Run 3 (0.025 h^{-1}; PFD = 163 µmol $\cdot m^{-2}$ $\cdot s^{-1}$) Run 4 (0.025 h^{-1}; PFD = 932 µmol$\cdot$ m^{-2} $\cdot s^{-1}$) and Run 5 (0.01 h^{-1}; PFD = 932 µmol$\cdot m^{-2}\cdot s^{-1}$.
B. Depicts results of Run 6 (0.025 h^{-1}; PFD = 932 µmol$\cdot m^{-2}\cdot s^{-1}$), Run 7 (0.014 h^{-1}; PFD = 1472 µmol $\cdot m^{-2}$ $\cdot s^{-1}$), the culture behaviour during photoinhibition and the recovery process until last Run 8 (0.025 h^{-1}; PFD = 932 µmol $\cdot m^{-2}\cdot s^{-1}$).

a maximum light power, from 1473 (Run 7) to 1700 µmol m^{-2} s^{-1}, and *D* is as well increased from 0.014 to 0.025 h^{-1}. In Run 7b, the r_{O_2} shows a progressive decrease from 1.00 to 0.88 mmol l^{-1} h^{-1} (Table 2) with no stabilization, even after six HRT. The initial decrease of biomass was expected because of higher *D,* but a steady condition is never reached. A minimum cell density of 0.66 g l^{-1} is reached during this condition. However, the dynamics regarding r_{O_2} differs from the expected results and shows a decline. Stabilization of oxygen production is never achieved, and all evidences make clear the photoinhibition phenomena: biomass wash out, r_{O_2} drop, impossibility to reach steady state and culture appearance. In Run 7b, the r_{O_2} shows a progressive decrease from 1.00 to 0.88 mmol l^{-1} h^{-1} (Table 2) with no stabilization, even after six HRT. On day 137, *D* was set at 0.025 h^{-1} and PFD at 1700 µmol m^{-2} s^{-1}. The initial decrease of r_{O_2} was expected because of higher *D,* but a steady condition was never reached. Indeed, during those days the broth shows a yellowish colour (data not shown), which is an indication of pigment degradation.

In order to investigate if this photoinhibition event was reversible, on day 152, light was decreased to 390 µmol m^{-2} s^{-1} while *D* was kept at 0.025 h^{-1}. As presented in Fig. 1, the negative effect on r_{O_2} and cell density is still occurring and stability is not achieved (from day 151 to day 164). True culture recovery only occurs when the bioreactor is switched to batch operation mode (from day 164 to day 171) and PFD is set at a low value of 150 µmol m^{-2} s^{-1}. No immediate response is observed on r_{O_2} and biomass for the first two days, but a significant change is appreciated in culture colour (from yellowish to green), which is a clear indication of higher pigment content. Recovery of cell concentration and r_{O_2} takes place after further increasing the PFD to 300 µmol m^{-2} s^{-1}. The confirmation of recovery from photoinhibition is obtained when biomass reaches 1 g l^{-1}, run 8 is started (PFD 932 µmol m^{-2} s^{-1}; *D* 0.025 h^{-1}) and stability is reached after one HRT and maintained during three additional HRT. In this condition, r_{O_2} reaches 1.22 $\pm$ 0.03 mmol l^{-1} h^{-1} and is not statistically different ($P > 0.05$) than average $\overline{r}_{O_2}$ from Runs 1, 4 and 6.

Table 2. Biomass concentration, oxygen production and carbon consumption rates results obtained in steady state for each experimental condition.

Run	PFD ($\mu mol \cdot m^{-2} \cdot s^{-1}$)	D (h^{-1})	X ($g\ l^{-1}$)	qPFD ($\mu mol \cdot g^{-1} \cdot s^{-1}$)	r_{O_2} ($mmol \cdot l^{-1} \cdot h^{-1}$)	q_{O_2} ($mmol \cdot g^{-1} \cdot h^{-1}$)	r_{CO_2} ($mmol \cdot l^{-1} \cdot h^{-1}$)	q_{CO_2} ($mmol \cdot g^{-1} \cdot h^{-1}$)	PQ ($mol_{O2} \cdot mol_{CO2}^{-1}$)
1	**932**	**0.025**	1.05 ± 0.07	15.14	1.35 ± 0.04	1.29 ± 0.12	−1.00	−0.86	1.40
2	**387**	**0.014**	1.07 ± 0.04	6.12	0.73 ± 0.04	0.62 ± 0.06	−0.59	−0.49	1.25
3	**163**	**0.025**	0.32 ± 0.02	8.63	0.40 ± 0.02	1.13 ± 0.12	−0.27	−0.75	1.50
4	**932**	**0.025**	0.90 ± 0.04	17.56	1.14 ± 0.03	0.99 ± 0.08	−0.92	−0.80	1.24
5	**932**	**0.010**	1.65 ± 0.10	9.59	0.93 ± 0.03	0.41 ± 0.06	−0.73	−0.32	1.27
6	**932**	**0.025**	0.82 ± 0.01	19.22	1.06 ± 0.03	0.95 ± 0.05	−0.77	−0.69	1.37
7	**1472**	**0.014**	1.42 ± 0.05	17.61	1.14 ± 0.03	0.81 ± 0.06	−0.97	−0.68	1.19
7b[a]	**1700**	**0.025**	0.71–0.94	30.6–40.6	0.88–1.00	1.24–1.19	−0.68–(−0.75)	−0.96–(−0.89)	1.29–1.33
8	**932**	**0.025**	1.01 ± 0.02	15.64	1.22 ± 0.03	1.20 ± 0.05	−1.07	−1.06	1.14

Runs highlighted in grew correspond to the repeated condition.
[a]Results from condition 7b are not obtained from the steady state, but the range of values resulted from the condition are displayed. Steady state was never reached on 7b because of photoinhibition.
Columns corresponding to manipulated variables are highlighted in bold

L. indica *composition*

Table 3 presents the cell composition corresponding to each steady state condition in the PBR operation as previously described. It focuses on pigments, protein and CH content.

A wide range of pigment content is obtained along the experiments for both PBPs and Chl *a*. The highest PBPs content, 12.5%, is obtained for a qPFD of 6.1 $\mu mol\ g^{-1} s^{-1}$. The lowest PBP, 3.7%, is obtained for a qPFD of 17.6 $\mu mol\ g^{-1}\ s^{-1}$. Same behaviour is observed for Chl *a* with a maximum of 1.8% (qPFD 6.1 $\mu mol\ g^{-1}\ s^{-1}$) and a minimum of 0.7%–0.8% (qPFD 17.6–19.2 $\mu mol\ g^{-1} s^{-1}$). Carotenoid content ranges between 0.4% and 0.7%, but it shows a lower influence by light. Correlation between qPFD and pigment content has been statistically analysed based on Pearson's correlation. There is a strong negative correlation between PBPs content and qPFD ($r = -0.888$; $P < 0.05$). The same is observed for Chl *a* content even at a stronger correlation ($r = -0.936$; $P < 0.001$). Carotenoids do not show a significant correlation with qPFD ($r = -0.681$; $P > 0.05$).

Among all PBPs, the main pigments generally found in *L. indica* were analysed (PC, APC, PE). The most abundant is PC representing in all conditions between 73% and 77% of the total PBPs composition, followed by APC ranging from 20% to 24% of total PBPs. PE presence is reduced to a level of 1%–4% of total PBPs. *L. indica* is reported to reach PC, APC and PE content up to 17%, 4% and 1% respectively (Bhattacharya and Shivaprakash, 2005; Patel *et al*., 2005; Chen *et al*., 2010). Additionally, no differences are found in the PC/APC ratio, which is maintained between 3.1 and 3.9, in agreement with previous reported data (Vonshak, 2002).

Special attention is focused on the dynamics of the system during transition phases or conditions were steady state is not reached. Figure 2 displays the evolution of cell composition during the 177 day experimental period. *Chla* and PBPs both follows the same behaviour. It is in agreement with the negative Pearson's correlation values previously obtained. The period between days 140 and 165 shows the lowest pigment content for PBPs and Chl *a*. It coincides with previously reported photoinhibition period. Lowest content values for PBPs and Chl *a* are 0.76% and 0.58%, respectively, in day 161. At this moment, culture colour looks yellow-like (data not shown) suggesting pigments degradation. Recovery of pigment content is observed 24 h after decreasing the PFD from 386 to 150 $\mu mol\ m^{-2}\ s^{-1}$. PBPs increases from 1% to 3.88%, and Chl *a* +carotenoids changes from 0.8% to 1.1%. At the end of the recovery phase, on day 171, PBPs and Chl *a* +caroteniods content reaches 11.3% and 2.51% respectively.

Table 3. Cell composition of *L. indica* for each steady state condition.

Run	PFD (μmol m^{-2} s^{-1})	qPFD (μmol·g^{-1} s^{-1})	PC (%)	APC (%)	PE (%)	PC/APC	PC/PE	PBPs (%)	Chl *a* (%)	Carot. (%)	Protein (%)	CH (%)	PBP/Prot (%)
2	387	6.12	9.2 ± 0.7	3.0 ± 0.4	0.2 ± 0.0	3.1	41.3	12.5 ± 0.9	1.8 ± 0.1	0.6 ± 0.1	55.6 ± 4.2	13.0 ± 1.2	22.4
3	163	8.63	7.5 ± 0.6	2.0 ± 0.4	0.2 ± 0.0	3.7	32.7	9.8 ± 0.2	1.6 ± 0.2	0.6 ± 0.1	49.2 ± 1.6	13.6 ± 1.2	19.9
4	932	17.56	2.9 ± 0.4	0.7 ± 0.2	0.1 ± 0.1	3.9	25.6	3.7 ± 0.6	0.7 ± 0.1	0.4 ± 0.1	42.5 ± 2.5	24.6 ± 2.4	8.8
5	932	9.59	8.4 ± 0.6	2.5 ± 0.2	0.3 ± 0.1	3.3	32.9	11.1 ± 0.6	1.4 ± 0.0	0.7 ± 0.1	47.9 ± 4.3	15.9 ± 1.8	23.2
6	932	19.22	3.4 ± 0.2	1.1 ± 0.1	0.2 ± 0.0	3.2	18.7	4.7 ± 0.3	0.8 ± 0.0	0.5 ± 0.0	42.0 ± 3.8	24.6 ± 1.2	11.1
7	1473	17.61	6.1 ± 0.5	1.7 ± 0.1	0.3 ± 0.0	3.6	21.4	8.1 ± 0.6	1.1 ± 0.0	0.6 ± 0.0	47.3 ± 1.0	19.6 ± 0.8	17.2
8	932	15.64	6.2 ± 0.4	1.8 ± 0.3	0.2 ± 0.1	3.4	30.6	8.2 ± 0.2	1.2 ± 0.0	0.5 ± 0.0	47.9 ± 2.1	24.0 ± 1.2	17.2

Values of pigment content (PBPs, chlorophyll and carotenoids), protein and CH are reported. Pigment results for Run #1 are not shown due to the tuning of the analysis methodology.

Average protein and CH content for each steady state is presented in Table 3. Protein content ranges from 42% to 55% depending on the condition. These results are in agreement with previous work reporting protein content between 40% and 70% (Ciferri, 1983; Vonshak, 2002; Masot, 2007). The highest value is obtained for Run 7 (PFD 1472 μmol m^{-2} s^{-1}; *D* 0.014 h^{-1}), while the lowest content is found in Run 6 (PFD 932 μmol m^{-2} s^{-1}; *D* 0.025 h^{-1}). A statistical significant correlation (Pearson's method) between protein content and qPFD is found ($r = -0.82$; $P < 0.05$). Maximum and minimum PBPs fraction are 23% and 8.8%, respectively, which is considerably lower than theoretical maximum of 50% out of total protein. This can be explained by the relatively low phycobiliprotein content (maximum of 12% for Run 2). Regarding CH content, the opposite behaviour than protein is observed. High qPFD results in higher carbohydrate amounts. Maximum carbohydrate content is 24.6% and corresponds to the maximum qPFD of 19.2 μmol m^{-2} s^{-1}. The lowest CH content is 13% when qPFD is 6.12 μmol g^{-1} s^{-1}. Evidence of correlation between qPFD and CH content is found ($r = 0.925$; $P < 0.05$). Values are in accordance to previously reported content of 10%–20% (Ciferri, 1983; De Oliveira *et al.*, 1999).

Cell morphology characterization and CDW/OD ratio

On-line monitoring of cell density was performed during the 180 days experimental period. Figure 3 shows the evolution of off-line absorbance, off-line CDW and the optical biomass sensor signal (Dencytee®, Hamilton Company, Bonaduz, Switzerland). The optimal performance of the optical biomass sensor is proved by the very accurate fitting between off-line and on-line absorbance values. In most cases, there is a good correlation between optical measurement and off-line cell densities, but a deviation in respect to cell density is observed in some specific conditions. Among the different steady state conditions, the highest CDW/OD ratio of 0.99 ± 0.01 is obtained for Run 1. If all the test is considered (not only steady states), the highest CDW/OD ratio value is observed in the transition phase (between days 152 and 161) with a value of 1.00 ± 0.05. The lowest ratio value is observed in Run 7 with 0.67 ± 0.01. Average ratio during batch phase is maintained at 1.05 ± 0.04. According to the last results evaluation, CDW/OD ratio might depend on cell density. High cell densities results in lower ratio and low cell densities results in higher ratios values ($r = -0.61$; $P = 0.047$).

Microscopic observations enabled to obtain the distributions of characteristic size parameters (Fig. 5) at different culture conditions (*L: trichome Length; W: trichome Width; C: coil counts; P: pitch*). These results

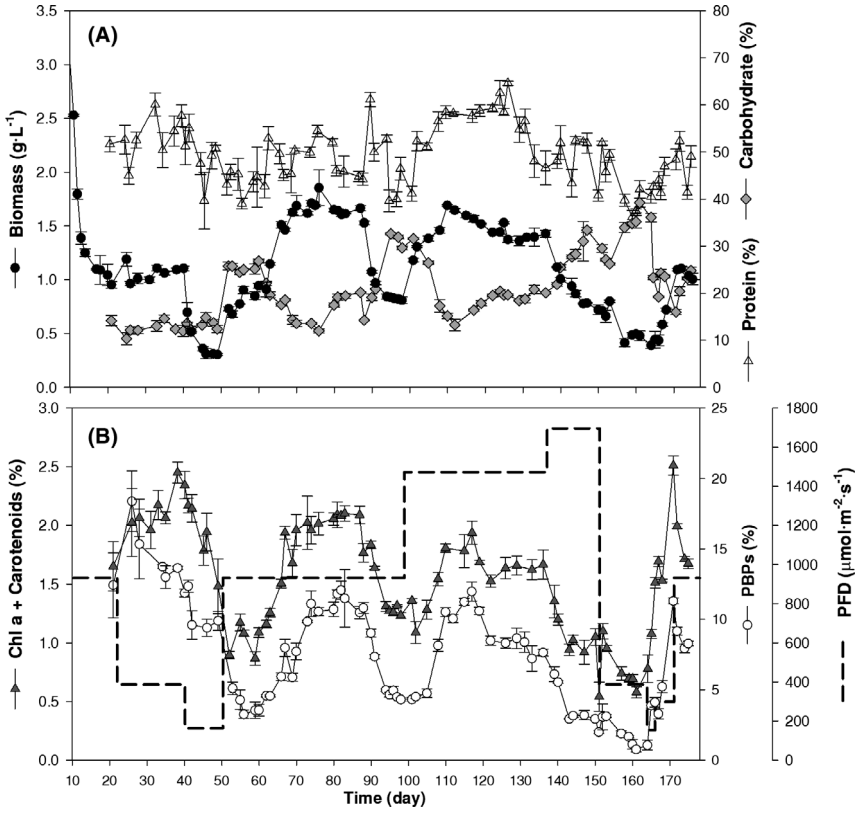

Fig. 2. Evolution of cellular composition of L.indica during continuous cultivation mainly affected by cell density and light intensity (PFD).
A. Shows the composition based on protein and carbohydrate content.
B. Focuses on pigment content: PBPs and chlorophyll. Content of *Chl a* and carotenoids is presented together.

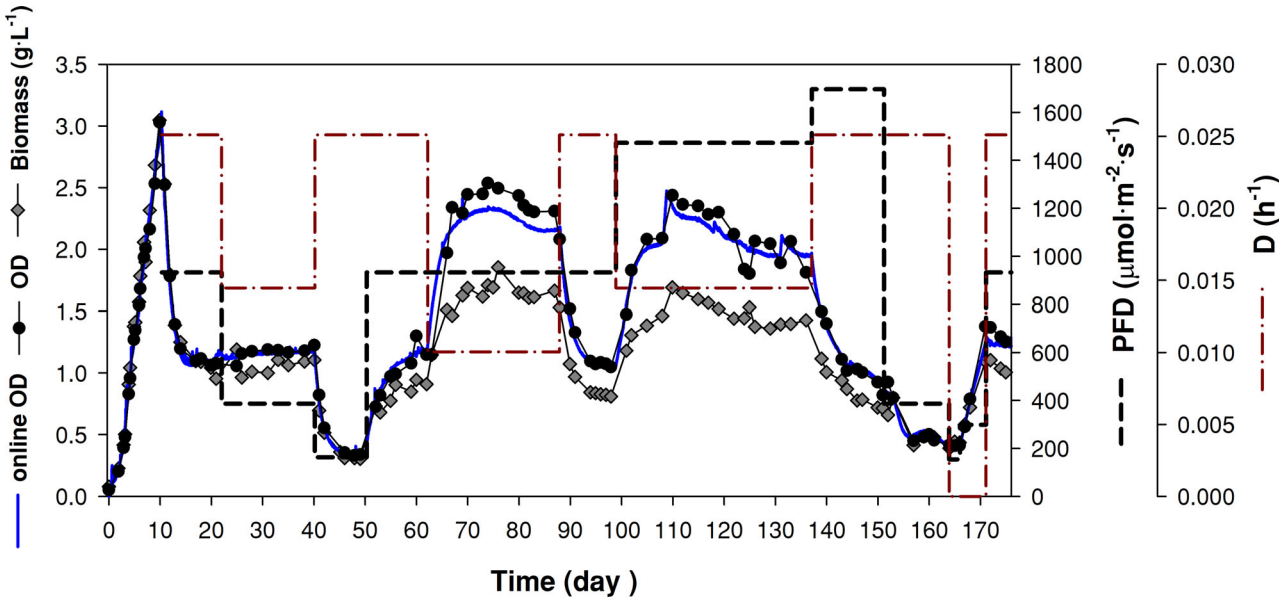

Fig. 3. Changes in CDW/OD ratio observed from off-line and on-line cell density analysis. Ratio is not maintained constant and absorbance cell dry weight values differs depending on tested condition. Initial period (1–10 days) corresponds to batch phase after inoculation.

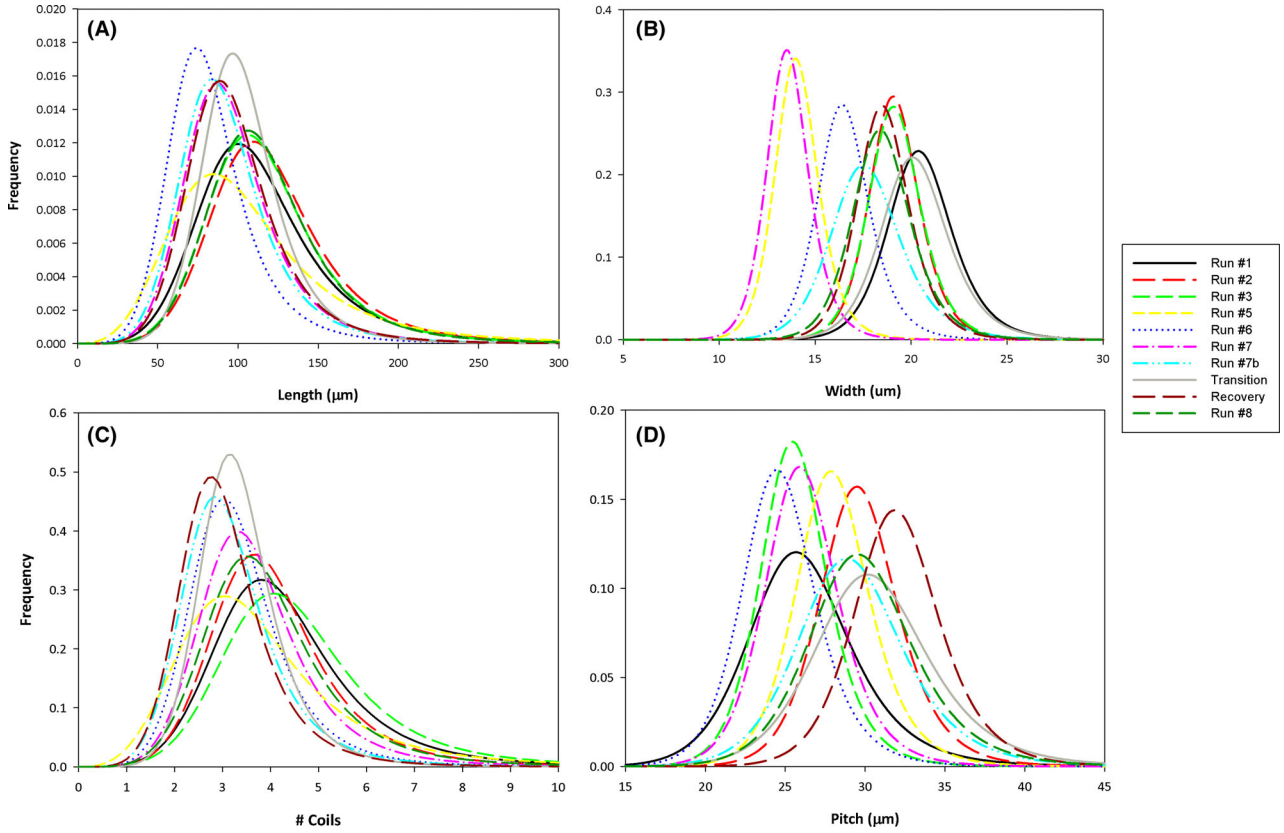

Fig. 4. Normalised cell size distributions for different parameters estimated from fitting Equation (12) with experimental measurements. Distributions correspond to trichome *Length* (A), trichome *Width* (B), coil *Counts* (C) and *Pitch* (D), and are obtained from steady states of each run. *Run 7b*, Transition and Recovery are representative from periods with photoinhibition (*Run 7b* and *Transition*) and recovery (*Recovery*). Run 4 data is not available.

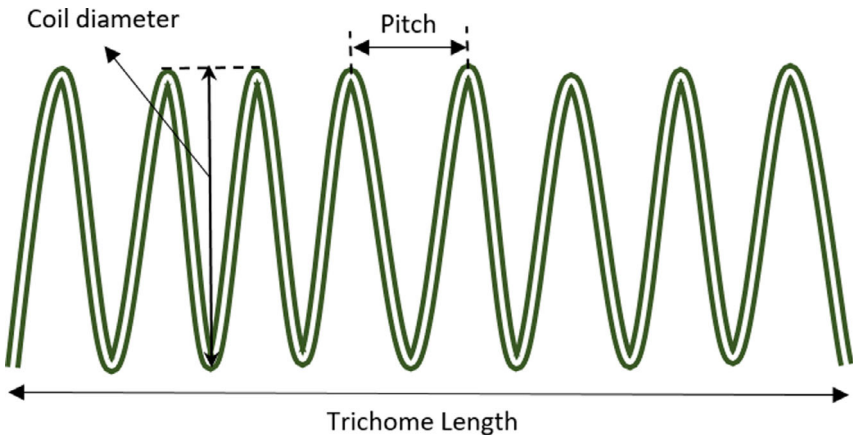

Fig. 5. Illustration of morphological parameters in *L.indica*. Helix Pitch is considered as the distance between two consecutive coils. Real determination of this parameter is performed dividing the length of the trichome by the number of coil turns.

are presented in Fig. 4 for each steady state condition and for additional conditions. *Run 7b* refers to period where cells were exposed to maximum PFD (1700 μmol m^{-2} s^{-1}) and photoinhibition was observed (time = 137–151 days); *Transition* corresponds to the period where the culture was exposed to lower PFD (386 μmol m^{-2} s^{-1}) during photoinhibition (t = 151–164 days); *Recovery* corresponds to the batch period (t = 164–171 days) where photoinhibition was reversed at 150 μmol m^{-2} s^{-1}. Trichome *Length* (Fig. 4A) shows

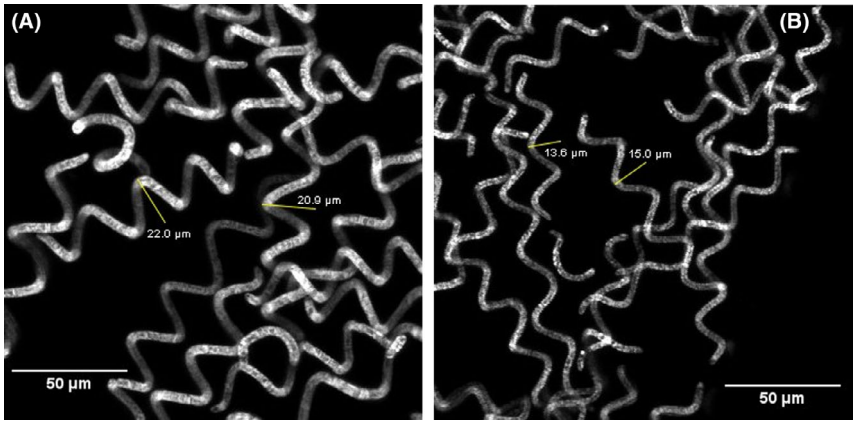

Fig. 6. Z-projections from confocal microscope slices obtained from Run 1 (A), Run 7 (B). Average coil width obtained from size distribution analysis is 20.5 and 13.6 respectively. These values were calculated from 120 cells obtained from different optical fields.

a similar distribution for each condition. *k* values (indicating the area attained by 50% of the population) ranges between 89.6 μm (Run 7b) and 117.2 μm (Run 2). The highest trichome length is observed for the initial period [Run 1 (k = 109 μm), 2 (k = 117 μm), 3 (k = 114 μm)]. No significant differences in trichome *Length* are found between these three conditions ($P > 0.05$). Afterwards, a decrease is observed for Run 5 (k = 98.5 μm) and the minimum value is observed in Run 6 (k = 79.6 μm), followed by a recovery for Run #7 until *Recovery* phase. Again, no significant differences are observed between Runs 7, 7b, *Transient phase* and *Recovery phase* ($P > 0.05$). Finally, *Trichome Length* is recovered to initial levels (k = 113 μm) for Run 8. Bibliographical values for *Trichome Length* can reach up to 3000 μm in some outdoors cultivated strains, with a minimum of 100 μm (Wu *et al*., 2005; Cheng *et al*., 2018). *Trichome Width* distribution is presented in (Fig. 4B). The highest *Trichome Width* results correspond to Run 1 (k = 20.5 μm). Similar values are obtained in Runs 2 and 3, where k = 19 μm in both cases. Then, a drastic decrease is observed as distribution moves to lower values. Lowest *k* occurs for Run 5 (k = 14.1 μm) and Run 7 (k = 13.6 μm). Finally, at the end of the experiment (*Run 7b*, *Transition*, *Recovery* and Run 8), the distribution recovers the initial *Width*. Reported values for *Trichome Width* in *L. indica* can be found between 20 and 100 μm (Kaggwa *et al*., 2013), or even lower values (7–11 μm) in some strains (Mühling *et al*., 2003). A third interesting parameter is the *Coil Counts*. A similar pattern than that observed for *Trichome Length* occurs for *Coil Counts* (Fig. 4C). Highest counts are observed in Runs 1, 2, 3 (k = 4.1; k = 3.9; k = 4.4). Afterwards, coil counts slightly drops from Run 6 up to *Recovery phase* showing significant differences in the results than in the initial scenarios ($P < 0.05$). At the end of the experiment (Run 8) coil *Coil Counts* recovers its initial value range (k = 3.8). The last important parameter is the *Pitch* size, which is the distance between two consecutives coils. An opposite pattern than the rest of parameters is observed. Lower *Pitch* is measured during the starting conditions than at the end of the experiment. The lowest value is observed in Run 6 (k = 24.7 μm). From that moment onwards a progressive increase is observed until reaching a maximum of k = 32.0 μm during *Recovery* condition. Typical reported values of *Pitch* range from 10 to 150 μm, (Wu *et al*., 2005) so the observed data shows that *Limnospira* strain used here is in the low range for *Pitch* size

The influence of previous parameters in CDW/OD ratio was further analysed by a Person's correlation approach. The only parameter that shows a significant influence on CDW/OD ratio is the *Trichome Width* ($r = 0.935$; $P < 0.001$). Fitting of CDW/OD ratio with *k* values of each size parameter are provided in Supporting Information (Fig. S3). A linear correlation is observed. Higher ratios are positively correlated with higher *k* values for *Trichome Width*, meaning that wider trichomes causes CDW/OD ratio to increase. Difference in *Trichome Width* is also evident in Fig. 6. It shows z-projection images from confocal microscope that had been used during the analysis. Trichome coil in image A is clearly wider than in B. A corresponds to Run 1 with k = 20.5 μm, while B corresponds to Run 7 with k = 13.6 μm. No significant correlation is found between any other parameter and CDW/OD ratio ($P > 0.05$). In relation to the parameter responsible of CDW/OD ratio variability, which it is trichome *Width,* it shows a significant correlation with cell density ($r = -0.7$; $P = 0.024$). Wider coils coincide with lower cell densities.

The effect of the different process conditions on the cell size parameters has been further analysed. Special attention has been focused on qPFD, PFD and cell density. Correlation study between variables indicates that no significance correlation is found between PFD and

any size parameters. There is no linear correlation (*Pearson's correlation*) between qPFD and any size parameters also ($P > 0.05$ in all cases). On the contrary, a non-linear significant correlation (*Spearman's rho*) is found between qPFD and *Length* ($P < 0.05$). Higher qPFD is correlated with lower trichome length.

Discussion

The obtained results evidence that *D* and PFD affect the performance of the studied PBR in terms of O_2 and biomass production. The continuous operation of the PBR was very stable and robust in the range of *D* from 0.01 to 0.025 h^{-1}, illumination of 163–1472 μmol m^{-2} s^{-1}. However, the performance can differ for a given condition in a different time period. This finding suggests that conditions experienced by the cells in a given period of operation have an effect on culture performance in the next period of operation. Indeed, similar phenomena have been observed in bacterial (Silva *et al.*, 2015) or mammalian cell cultures (Mulukutla *et al.*, 2015; Yongky *et al.*, 2015), and has been described as steady-state multiplicity. It is generally related to the metabolic state of the cells and can be directly affected by the intracellular concentration of metabolic enzymes that are determined by the past metabolic status of the cells. A new term, qPFD, is identified as the key parameter governing light availability to the cells. Our results prove that the cell culture exposed to high qPFD tends to decrease O_2 production rate in the next environmental condition. Such behaviour might be explained by downregulation of light-harvesting complexes under high qPFD (Muramatsu and Hihara, 2012) to avoid accumulation of ROS, which could have a counter effect on physiological state of the cell when shifting from high to lower qPFD exposure. Therefore, the observed results suggest that multiplicity of steady-state in continuous operation can also occur in the culture of cyanobacteria. To the best of our knowledge, this is the first time that such observation is made for cyanobacteria. Although no references have been found regarding steady-state multiplicity in cyanobacteria, a lot of work has been done regarding physiological responses of these microorganisms to environmental conditions. The most relevant are light changes, directly affecting growth rate and photosynthetic activity (Muramatsu and Hihara, 2012; Chakdar and Pabbi, 2015). In this sense, physiological state of the cells is reflected by pigment content (Table 3). Low pigment content is a response of the cell to high light energy absorbed to prevent formation of reactive oxygen species (ROS; Chakdar and Pabbi, 2015). As PFD and *D* are the same for Runs 1, 4, 6 and 8, the only factor that could explain such physiological differences is the dynamic of the system in transition phases from previous conditions.

Results also show the photoinhibition effect affecting the cells. It was observed at a cell concentration lower than 1 g l^{-1} (corresponding to a *D* of 0.025 h^{-1} and PFD of 1700 μmol m^{-2} s^{-1}) and a qPFD of 29 μmol g^{-1} s^{-1}or higher. From a kinetic point of view, a lot of research has been undertaken in the last 15 years to develop mathematical models for the prediction of volumetric rates of biomass production (Cornet *et al.*, 1998; Dauchet *et al.*, 2015; Charon *et al.*, 2016). It has been defined that cells can be under a '*Kinetic regime*' where r_X depends on cell concentration, or under '*Physical limitation regime*' where r_X depends on light availability (Cornet, 2007). In the first condition, part of the light is transmitted through the bioreactor volume and the transmittance value is > 0%. It is likely that last situation is the one taking place during the photoinhibition process. In this case, the high $P/2e^-$ ratio imposes constrains on cell metabolism leading to changes in biomass composition. $P/2e^-$ can even reach the theoretical limit of 1.7 when biomass growth is devoted only to exopolysaccharide (EPS) production. In the second condition ('*Physical limitation regime*') all the light is absorbed by the culture, so the volume illuminated fraction (γ) is < 1. Consequently, it is recommended to maintain a $P/2e^-$ ratio below 1.5, which is ensured by $\gamma < 1$(Cornet, 2007). An additional consequence of photoinhibition is the damage of photosystem II (PSII). As PSII is involved in H_2O photolysis (Z-scheme photosynthesis; Cogne *et al.*, 2003a), the macroscopic consequence is the r_{O_2} drop, which occurred here at the mentioned conditions (Run 7: PFD 1700 μmol m^{-2} s^{-1}; *D* 0.025 h^{-1}). Additionally, the fact that steady state could not be reached for Run 7 also supports the photoinhibition event.

Our findings also show that photoinhibition process can be reversible. The cells recovered when the culture was set in batch mode and PFD reduced to 150 μmol m^{-2} s^{-1} followed by a PFD 300 μmol m^{-2} s^{-1} after 2 days (Fig. 1B). Recovery of the cells was clearly observed in the last condition. Although this might seem a contradiction, it can be explained on the basis of the cell dynamics. Initially, cells were exposed to very dim light conditions (150 μmol m^{-2} s^{-1}). During these two days period (initial two days of the batch; days 164 and 165), reparation mechanisms would be active (Allakhverdiev *et al.*, 2005; Muramatsu and Hihara, 2012). However, at such low PFD cell growth might be physically limited by light until PFD is doubled on day 166 (from 150 to 300 μmol m^{-2} s^{-1}). Reversibility of the process is demonstrated during Run 8. O_2 production for this condition was not statically different than average production from other conditions with same experimental parameters (Runs 1, 4 and 6). It means that the performance of the PBR is within the range observed for previous periods under the same illumination and flow rate conditions.

Photoinhibition recovery was possible after switching the PBR to batch mode. Considering the context of the MELiSSA loop, it is characterized by uninterrupted operation of all the compartments in continuous mode. However, the fact that by exploring the limits of the operation we found photoinhibition that needed a batch mode operation time should not be read as that continuous operation cannot be maintained. It should be read as that continuous operation can be maintained by setting the operation conditions out from the inhibition zone. In case, by accident a photoinhibition conditions occurs, it is demonstrated that the biological system shows a recovery capacity that enables to resume the continuous operation after an interrupted period of batch.

From the described results, it is concluded that cells experienced photoinhibition in the PBR when growing at a concentration lower than 1.5 g l^{-1} and were exposed to high PFD (1700 μmol m^{-2} s^{-1}). Photoinhibition process in cyanobacteria, algae and higher plants has been widely studied due to the increased interest in culture intensification. It is known to be a complex mechanism where the critical step is the activation of PSII (Allakhverdiev *et al*., 2005). D1 is the main protein forming PSII. During photoinhibition, D1 protein is affected and provokes a functionality loss of PSII. However, this is reversible by *de novo* synthesis of D1 protein, resulting in a high rate turnover light-dependent process (Mattoo *et al*., 1989). Additionally, it has been demonstrated that low temperatures might delay PSII repair (Jensen and Knutsen, 1993). In our case, temperature is kept constant at 36°C, which might have helped in the recovery process.

Cell recovery from photoinhibition occurred at 150 μmol m^{-2} s^{-1}. This value is in the range of recommended minimal PFD values of 50 μmol m^{-2} s^{-1} (Jensen and Knutsen, 1993; Vonshak *et al*., 2000; Allakhverdiev *et al*., 2005). Success of recovery might be influenced as well by two elements. First, cells were not irreversibly inhibited, so regeneration of PSII was possible under such PFD considering 150 μmol m^{-2} s^{-1} is a relatively low value. Second, minimum cell density was 0.5 g l^{-1}, comparably higher than those reported for other photoinhibition studies. In the same direction, for a cell concentration of 0.17 g l^{-1} recovery from photoinhibition was possible at lower PFD than 150 μmol m^{-2} s^{-1} (Jensen and Knutsen, 1993). Therefore, the photoinhibition phenomenon is a complex mechanism where both the light intensity and cell concentration are influencing parameters. From the PBR operational point of view, the main conclusion from the photoinhibition disturbance experienced is that it must be ensured that the process operates under a '*Physical limited regime*' and all incident light is absorbed by the culture.

As discussed previously, what really influences the behaviour of cyanobacteria under different light intensities is light availability rather than the amount of light. Light availability is directly proportional to the amount of light and inversely proportional to the amount of cells. Hence, it was considered that for better understanding of cell composition changes, qPFD is more suitable. Results described in Table 3 regarding CH and pigments content together with correlations found between them and qPFD corroborate that the main physiological response of the cells to changes in light availability is the regulation of the mechanisms elements related to light absorption. This response aims to protect the cell from the generation of ROS and from an excess of generated energy ($P/2e^{-}$). Decrease in Chl *a* is directly related to the downregulation of PS I, as it accounts for 80% of the total Chl *a* (Weiwen Zhang, 2018), while decrease in PBPs is linked to the downregulation of genes encoding for PBS subunits (Muramatsu and Hihara, 2012; Weiwen Zhang, 2018). Irreversibility of photoinhibition was probably avoided thanks to the biological regulation of PSI content. It is known that cyanobacteria downregulate their PSI content to avoid the generation of significant amounts of ROS under high light (Muramatsu and Hihara, 2012), as confirmed by a lower Chl *a* content. A second factor that might have contributed is the PFD value attained. In our case, PFD maximum value was 1700 μmol m^{-2} s^{-1} when the photoinhibition was detected, compared with 2500 μmol m^{-2} s^{-1} for those cases where irreversible photoinhibition has been reported (Allakhverdiev *et al*., 2005). These results show the importance of analysing cell composition related to specific PFD rather than absolute PFD. For example, when comparing Runs 4 and 5 PBPs content, it increases from 3.7% to 11.1% even the absolute PFD is maintained at 932 μmol m^{-2} s^{-1}. Indeed, this is caused by the change in *D* from 0.025 down to 0.01 h^{-1} provoking an increase in cell density and consequently, decreasing qPFD from 17.56 to 9.59 μmol g^{-1} s^{-1} respectively. The opposite effect was observed when reversing the conditions and a *D* of 0.025 h^{-1} was recovered in Run 6. In most studies there is a tendency to analyse the cell composition and all the regulation elements involved depending on light intensity. The effect of light availability has been mentioned by some authors studies (Rodríguez *et al*., 1991; Begum *et al*., 2016), but no quantitative analysis has been carried out. The light availability approach might be useful for transient phases where biomass concentration does not change significantly in a short time frame. However, when it comes to long-term operation in continuous PBRs, cell concentration changes are very relevant at different dilution rates. In closed-loop life support systems, there are different parameters to optimize: biomass production and composition, and O_2 production. In these continuous systems, if high PFD operation is fixed, it is possible to modulate

the biomass response by changing the dilution rate and, consequently, cell density.

Regarding pigment content, it followed the same trend as cell density, confirming the strong dependence of pigment synthesis with light availability (Fig. 2). In all transition phases, changes in pigment content were detected within 1 or 2 days after setting the new illumination or dilution conditions. Changes in molecular composition where not assessed in this transition phases, since effort was focussed on the analyses of steady-state conditions. However, there is evidence in the literature that response from *Limnospira* cells is reflected at composition level in < 5 h (Tomaselli *et al*., 1997). The lowest pigment content coincided with the photoinhibition phase. Their recovery was the first indication of cells recovery from photoinhibition. These observations support that cell composition is the first parameter to be affected before any change is observed at process level, as no response was still detected in r_{O_2} and cell density (Fig. 1 day 164 to day 166). Pigment content of the cells on day 171 confirmed the culture recovery from photoinhibition. The ratio between different types of PBPs showed that no significant differences were found in PC/APC (Table 3). Variability in PC/PE might be related to the analysis deviation caused by the lowest PE content, rather than changes in the ratio itself. Some authors have reported changes in the PC/APC ratio of *Synechocystis* due to changes in light intensity, mainly because of reduction of PC synthesis to drop antenna size (De Lorimier *et al*., 1992; Hihara *et al*., 2001). Other studies focused on *L. indica* do not suggest any significant variation in PC/APC ratio with light intensity (Nomsawai *et al*., 1999). This might indicate that changes in PC/APC ratio to light intensity are species dependent.

In order to discuss the results related to protein and CH content (Table 3), it is important is to consider the light availability, rather than absolute intensity. Our results are in agreement with literature, as the negative correlation obtained between qPFD and protein content proves the effect of low light availability, low qPFD, on protein content. Most authors found a clear effect of light intensity on protein content showing that high light intensities causes drops in protein synthesis (Tomaselli *et al*., 1997; Markou *et al*., 2012). Considering that PBPs content can account up to 50% of total protein (Nomsawai *et al*., 1999), a reduction in PBPs synthesis as observed here, should have been translated into a lower total protein content. However, the opposite result previously described could be explained by a significantly lower PBPs fraction out of total protein. Regarding CH, variation in CH content is normally related to stress conditions. Nutrient limitation such as nitrogen or phosphorus limitation, causes an increase of CH content as a way to increase carbon feedstock (Markou *et al*., 2012; Depraetere *et al*., 2015). In the presented results, the increase of CH cannot be related to nutrient limitation because nitrogen, phosphorous and sulphur were always in excess. CH content could be potentially affected by qPFD, since higher light availability causes accumulation of intracellular CHs. Some authors already observed this cell metabolic behaviour when comparing situations with low light or high light (Tomaselli *et al*., 1997). Under high light availability, resulting in a $P/2e^-$ ratio near 1.5, the cells triggers the accumulation of EPS. It is understood as a metabolic strategy to divert the energy excess of produced by photosynthesis. As EPS are formed by CHs (Ahmed *et al*., 2014), observing a high CH content under high light availability is consistent with the metabolism response of the cell described in the literature. From an evolutionary point of view, such accumulation during high light availability periods could serve as a feedstock for protein and pigment synthesis during low light availability and it would result in higher photosynthetic efficiency under light limiting conditions. However, these initial hypotheses should be further investigated.

We showed that changes in CDW/OD ratio occurs along the long-term cultivation. A significant negative correlation was found between CDW/OD ratio and cell densities. A possible explanation is the influence of cell density in off-line OD measurement. However, this hypothesis must be discarded because in the initial batch phase (from day 0 to day 11), the ratio was maintained constant at $R = 1.05$ independently of the cell density. The hypothesis proposed to understand this lack of fit is based on the fact that changes in cell morphology at different culture condition affect the radiative properties of the cell that are, in turn, reflected in the spectrophotometric determinations (Dauchet *et al*., 2015). In the presented results, *Width* was the responsible morphological parameter affecting the CDW/OD ratio. Aside from the statistical result, no biological explanation is found for this behaviour. From a radiative perspective, trichome *Width* showed an influence in scattering properties of the cells. In case of wider coils, more light is scattered and therefore, measured absorbance increases for the same cell density. Cell shape and size distribution have been identified as key aspects in finding the radiative properties of photosynthetic microorganisms (Pilon *et al*., 2011; Dauchet *et al*., 2015, 2016). In the case of *Limnospira,* more difficulties were found to obtain a radiative model that fits with experimental results (Dauchet *et al*., 2015) because of the spiral shape. However, in addition, we proved that light availability not only influences the biological activity of the cells, but it might also influence the trichome morphology. The influence of environmental conditions (light, temperature, salinity, pH, nutrients) on trichome morphology of *Limnospira* has been reported in the literature. The main parameters

affected by such variables are mainly the trichome length and the helix pitch, as a morphological response of cyanobacteria to stress conditions (Kaggwa *et al*., 2013; Ogato and Kifle, 2014). Long trichome is normally related to high vitality cells and growth rate, while short trichome is related to cells under stress conditions or limitations. An almost complete breakage of cells and helix pitch decrease when exposed to high solar radiation including UV-B for short (hours) and long periods (days) has been reported (Wu *et al*., 2005). However, this breakage was significantly reduced to 50% if UV-B is filtered out. Such effects were observed in the literature with cell density cultures between 0.33–0.78 g l^{-1}. In the presented study, reduction in trichome length was not drastic and, even that a correlation was found, the minimum length is 67% of the maximum. This observation is coherent with the conditions used in the current experiments, avoiding the UV region, and higher cell densities. Several authors have reported changes in helix pitch with exposure to high levels of solar radiation in open ponds or in natural environments (Kaggwa *et al*., 2013; Cheng *et al*., 2018). The data obtained in our work demonstrate that even cells were photoinhibited when exposed to high qPFD, this did not translate into significant morphology changes, except for a minor decrease in length. Additionally, spiral breakage is not clearly observed, which is consistent with the reversible photoinhibition process. In some studies, spiral breakage has been related to ROS accumulation (Ma and Gao, 2010). From a process point of view, changes in trichome morphology would present some implications in on-line cyanobacteria biomass monitoring techniques. On-line biomass monitoring is proved to be valid when morphological properties of the cells are maintained. If variations in such properties occurs, then the on-line values might be corrected with the information from off-line CDW/OD ratios. Additionally, optical based techniques can be complemented with sensors based on media permittivity, such as capacitance probes (Kiss and Németh, 2016). Hence, the use of different technology based sensors could provide information about changes in cell morphology.

The characterization of the continuous air-lift PBR demonstrates the role played by the two main operational variables, PFD and dilution rate, in the reactor performance. The identification of qPFD as an indication of light availability allows to understand and predict the biological behaviour of the cells in the various experimental conditions tested. Moreover, it has also resulted as a key parameter determining the operational limits of the PBR in order to avoid potential photoinhibition phenomena. This is a significant advance in the MELiSSA loop context, where robustness, reliability and reproducibility of biological systems is a must. In view of such possibilities, this scenario provides the opportunity to optimize the performance of *L. indica* continuous culture in closed-life support systems, where efficient processes for food production and air revitalization are needed. In addition to the importance of the presented work in the field of Life Support Systems in Space within the MELiSSA project, the knowledge generated in this research it is as well of interest beyond. The potential of photosynthetic processes and the associated bioreactor development are receiving increased interest in diverse applications ranging from added value chemicals production, functional food components, advanced waste treatment and biofuels, among others. Hence, the characterization of intensive illumination in PBRs described here could certainly be of general interest in many of these applications.

Experimental procedures

Pilot plant PBR description

A 83 l external-loop air-lift PBR was used for *L. indica* cultivation. Bioreactor construction details have been described in previous work (Alemany *et al*., 2019). It consists of two glass cylindrical sections of 15 cm diameter surrounded by a LED-based illumination system. For continuous operation of the bioreactor, the inlet feed medium was pumped by a variable speed gear pump (Lewa, EEC0002S11, Hispania S.L., Leonberg, Germany) followed by a 0.2 μm filtration (MCY4440DFLPH4, Pall Corporation, New York, NY, USA). Outlet flow is regulated with a variable speed peristaltic pump (Watson-Marlow 323Du, Watson Marlow Fluid Technology Group, Wilmington, NC, USA). Inlet and outlet air supply was regulated and measured by means of three flow-metres and controllers (Bronkhorst, F-202D-FA, Bronkhorst, Ruurlo, Netherlands).

Illumination system

PBR was illuminated by a specifically designed system (Intravision, Oslo, Norway) with a total of 16 LED lamps distributed around the two glass columns (eight lamps per column). Each lamp was composed of 80 cool white LEDs (LUXEON SunPlus 20 Line L1SP-CW90002000000; Lumileds, San Jose, CA, USA). Light intensity was regulated with a 0–10 V analogue signal connected to the drivers (EUD-600S140DV, Invertronics, China) providing a maximum electrical power of 2500 W. Light PAR (Photosynthetic Active Radiation; 400–700 nm) intensity was measured at the bioreactor surface, in the glass-liquid interface, with a plane cosine quantum sensor (Li-Cor 190R; Li-COR, Lincoln, NE, USA). A maximum PPFD (Photosynthetic Photon Flux Density) was 1700 μmol m^{-2} s^{-1}. Additional information

about the light intensity profile and light spectrum is described in Supporting information.

Cell strain, culture media and culture conditions

Limnospira indica PCC 8005 was provided by SCK CEN, Belgium. The strain was cultured in axenic conditions in continuous mode. A medium based on modified Zarrouk (Cogne *et al*., 2003b) was used. It consisted in a composition as follows: 2.5 g l^{-1} of $NaNO_3$, 1 g l^{-1} of K_2SO_4, 1 g l^{-1} of NaCl, 0.1 g l^{-1} of $MgSO_4{\cdot}7H_2O$, 0.04 g l^{-1} of $CaCl_2{\cdot}2H_2O$, 0.01 g l^{-1} of $FeSO_4{\cdot}7H_2O$, 0.08 g l^{-1} EDTA-2Na·$2H_2O$, 0.5 g l^{-1} K_2HPO_4, 0.18 g l^{-1} of $(NH_4)_6Mo_7O_2{\cdot}4H_2O$, 1.81 mg l^{-1} of $MnCl_2{\cdot}4H_2O$, 0.22 mg l^{-1} of $ZnSO_4{\cdot}7H_2O$ and 0.079 mg l^{-1} of $CuSO_4{\cdot}5H_2O$. Bioreactor was operated at 80 mbar overpressure. pH was controlled at 8.5 with the addition of NaOH (1 M) and of H_2SO_4 (1 M) as required. CO_2 was supplied by continuous gas injection at 2%–3% in order to maintain a TIC (total inorganic carbon) concentration above 200 ppm in the liquid phase. A set of dilution rates ranging from 0.01 to 0.025 h^{-1} and light intensities, from 150 to 1700 μmol m^{-2} s^{-1} were tested. Each condition was tested until reaching steady state.

Biomass concentration and optical density determination

On-line and off-line monitoring of biomass was carried out in parallel. An optical cell density probe (Dencytee®, Hamilton Company, Bonaduz, Switzerland) measuring at 880 nm was used for on-line absorbance monitoring. Biomass concentration was estimated off-line by cell dry weight (CDW) determination. Culture broth of 25–50 ml of were filtered through a 47 mm-glass microfibre (GMFC-52047, Scharlab, Barcelona, Spain), dried at 105°C until constant weight. Additionally, biomass was measured by optical density at 750 nm in an optical spectrophotometer (UV–vis DR6000, Hach, Düsseldorf, Germany).

TIC and nitrogen determination

Filtered fractions for biomass determination were used for NO_3^- and TIC analysis. Samples were diluted 1:100 with mili-Q H_2O and NO_3^- was analysed by spectrophotometry with LCK 339 kits (Hach, Germany). For TIC determination a 1:5 dilution with mili-Q H_2O was required; 1.5 ml of sample were loaded to a multi N/C2100S equipment (Analytik Jena, Germany). Two-hundred microlitres sample from the sample were injected into the acidic TIC reactor and 0.5 ml of H_3PO_4 at 10% were added to the chamber. CO_2 generated from the acidification was detected by the NDIR detector and quantified by triplicate.

Gas analysis, O_2 production and CO_2 consumption

Outlet gas composition from the PBR was measured on-line by an IR analyser for CO_2 coupled to a paramagnetic analyser for O_2 (600 series, CAI, USA). Oxygen volumetric production rate (g l^{-1} h^{-1}) was calculated on-line by the gas–gas-in–gas-out method:

$$r_{O_2} = (((F_{in} - F_{CO_2}) \cdot 0.2089 - (F_{out} \cdot O_{2out}/100))/22.4 \cdot MW_{O_2})/V_R \quad (1)$$

where F_{in} is the inlet air flow, F_{CO_2} is the inlet CO_2 flow, F_{out} is the total outlet gas flow, O_{2out} is the outlet concentration of O_2 in %, MW_{O2} is the molecular weight of O_2 (32 g mol^{-1}) and V_R is the PBR volume (83 l).

CO_2 consumption was calculated for each condition considering on-line gas analysis and off-line TIC concentration in the steady state. In such situation, no carbon accumulation takes place and CO_2 can be calculated in mmol l^{-1} h^{-1} by means of the following material balance:

$$r_{CO_2} = CO_{2Loutlet} - (CO_2\,gas\,transfer) \quad (2)$$

$$r_{CO_2} = C_{Lout} \cdot D + F_{in} \cdot 22.4(X_{COUT} - X_{CIN}) \quad (3)$$

where C_{LOUT} is the carbon concentration (mmol l^{-1}) in the liquid outlet converted into CO_2 by means of molecular weight, D is the dilution rate (h^{-1}), F_{in} (l h^{-1}) is the bioreactor gas flow rate, X_{COUT} is the molar fraction of CO_2 in the outlet gas and X_{CIN} is the molar fraction of CO_2 in the inlet gas.

Cell composition

Pigment, protein and carbohydrate (CH) content were measured in every sample. Pigment analysis, including phycobiliproteins (PBPs), chlorophyll (Chl *a*) and carotenoids, was based on extraction and spectrophotometry measures as follows.

Phycobiliproteins. Phycobiliproteins concentration was estimated based on the method previously reported by (Patel *et al*., 2005), with some changes. Fresh biomass samples (by triplicate) were diluted to reach a concentration in the range of 0.5 g l^{-1} in a final volume of 15 ml. Cell suspension was further submitted to two cycles of flash freezing in liquid N_2 followed by thawing in a water bath at 37°C. Samples were incubated 1 h in the dark under very soft mixing after adding a concentrated $CaCl_2$ solution to reach a biomass-$CaCl_2$ ratio of 1:12 (g g^{-1}). Two millilitre of sample are collected for Chl *a* measurement. The rest of the sample was incubated one extra hour without agitation. Finally, 2 ml of sample were centrifuged at 10 000 *g* for 1 min at 4°C (accuSpin Micro 17, FisherScientific, Hampton, VA, USA) and the supernatant was collected and filtered through a 0.2 μm filter (Millex; MerkMillipore, Burlington, MA, USA) to remove any residual debris. The absorbance of

phycobiliproteins in the supernatant was measured on a UV–vis Spectrophotometer (DR6000, Hach) at wavelengths of 562, 615 and 652 nm. C-PC (C-phycocyanin), APC (Allophycocyanin) and PE (Phycoerythrin) concentration were calculated using the following equations respectively (Bennett and Bogorad, 1973).

$$\mathrm{PC}\,(\mathrm{g}\cdot\mathrm{l}^{-1}) = (A_{615} - 0.474\cdot A_{652})/5.34 \quad (4)$$

$$\mathrm{APC}\,(\mathrm{g}\cdot\mathrm{l}^{-1}) = (A_{652} - 0.208\cdot A_{615})/5.09 \quad (5)$$

$$\mathrm{PE}\,(\mathrm{g}\cdot\mathrm{l}^{-1}) = (A_{562} - 2.41\cdot \mathrm{PC} - 0.849\cdot \mathrm{APC})/9.62 \quad (6)$$

Chlorophylls. Samples collected in the previous procedure after 1 h of incubation were centrifuged at 10 000*g* for 1 min at 4°C, the supernatant was discarded and the pellet was resuspended with 80% acetone solution until no biomass particles were observed. Samples were centrifuged again at 10 000*g* for 1 min at 4°C (accuSpin Micro 17, FisherScientific) and the supernatant absorbance was read at 470, 647 and 664 nm. Acetone at 80% was used as a reference. Chl *a* and carotenoid content were estimated using the following equations (Wellburn, 1994; Porra, 2002):

$$\mathrm{Chl}\,a\,(\mathrm{mg}\cdot\mathrm{l}^{-1}) = 11.78\cdot A_{664} - 2.29\cdot A_{647} \quad (7)$$

$$\mathrm{chl}\,b\,(\mathrm{mg}\cdot\mathrm{l}^{-1}) = 20.05\cdot A_{647} - 4.77\cdot A_{664} \quad (8)$$

$$\mathrm{carotenoids}\,(\mathrm{mg}\cdot\mathrm{l}^{-1}) = (1000\cdot A_{470} - 1.82\cdot \mathrm{chl}\,a 85.02\cdot \mathrm{chl}\,b)/198 \quad (9)$$

Proteins. Protein content was determined by a modified Lowry method (Masot, 2007). All analyses were performed on lyophilized biomass, which was diluted with water to reach 1 g l^{-1} initial cell concentration. NaOH of 0.1 ml of 1N was added to 0.1 ml of cell suspension and incubated for 10 min at 100°C. Samples were then immediately cooled down and 1 ml of a reagent, prepared with 50 ml of 5% Na_2CO_3 and 2 ml of 0.5% $CuSO_4{\cdot}5H_2O$ in 1% sodium potassium tartrate, was added and mixed. One millilitre of 1N Folin-Ciocalteu reagent was added and incubated in the dark for 30 min. Standard solutions prepared with BSA (0–800 mg l^{-1}) underwent the same procedure. Optical densities were read at 750 nm (DR6000, Hach).

Carbohydrates. Total CHs were analysed by the phenol-sulphuric method (Herbert *et al.*, 1971). A biomass suspension with a final concentration of 0.5 g l^{-1} was prepared from lyophilized biomass. Phenol of 0.2 ml at 5% was added to 0.2 ml of suspension, followed by the addition of 1 ml of H_2SO_4 96%. Samples were incubated for 10 min at room temperature and absorbance read at 488 nm (DR6000, Hach). Standard solutions prepared with glucose (0–100 mg l^{-1}) underwent the same procedure.

Microscopic analysis

For each experimental condition, cell samples from the steady state were collected for microscopic observation by means of CLSM (Confocal Laser Scanning Microscopy). CLSM was performed with a Leica TCS-SP5 (Leica Microsystems Heidelberg GmbH, Mannheim, Germany) using the 63× (1.3 NA) plan apochromat oil immersion objective. Red autoflorescence from thylakoids was detected in the red channel (630–725 nm) using one laser diode (561 nm). Twenty microlitres of fresh samples were mounted on MatTek culture dishes (MatTec Corp., Ashland, MA, USA). Fluorescence was measured in *x*–*y*–*z* planes every 0.5 μm along the vertical axis with 1 Airy confocal pinhole. Projections were generated by the Fiji (ImageJ 1.52) software (National Institutes of Health, Bethesda, MD, USA) for 3D reconstructions by summing the intensities from all the z-planes. These projections were used for measuring the size parameters with the same software: length of the trichome, number of coils and diameter of coils.

Size distribution analysis

Different size parameters were analysed from microscopic images. A minimum of 120 cell counts were considered for each sample in order to obtain a representative estimation of the real distribution. Analysis did not only include steady state of each condition, but also included samples during photoinhibition period and recovery phase. The cell size parameters were fitted to a classic S-type curve. Then, the normalized cumulative cell distribution *S* was represented by the following equation:

$$S = x^a/(k^a + x^a) \quad (10)$$

where *S* is the cumulative cell parameter distribution, *x* is the corresponding size parameter, *k* is the 'half saturation constant' that indicates that half of the population is under that value and *a* indicates the spread of the distribution (higher *a* values indicate a narrower distribution). Determination of *a* and *k* parameters for each sample was done by fitting experimental results to Equation (10) with Solver function (Excel, Microsoft Corporation, Redmond, WA, USA). The derivative of the previous equation gives the cell distribution and frequency for a specific size as a continuous function.

$$s = \mathrm{d}S/\mathrm{d}x \quad (11)$$

$$s = (a\cdot x^{(a-1)}\cdot k^a)/(k^a + x^a)^2 \quad (12)$$

Constants *a* and *k* were found for each size parameter. Distribution was obtained for trichome *length* (*L*), trichome *width* (*W*), coil *count* (*C*) and *pitch* size (*P*).

Statistical analysis

One-way ANOVA analysis assuming differences in variances was performed to assess O_2 production results from repeated conditions (Runs 1, 4, 6 and 8 as further described in the Results section). A significance value of $P < 0.05$ was considered. Data did not follow a normal distribution, but no transformation was needed as large number of samples from each condition was used. Games-Howell method (with a level of significance $P = 0.05$) was used for multiple comparison after one-way ANOVA analysis of the four types of size parameters. Pearson's correlation was used to study the influence of past qPFD on current O_2 production values with a level of significance $P < 0.05$. The same correlation analysis was performed with the molecular composition of the cell with a level of significance $P = 0.05$, where the influence of light availability on pigments, protein and CH content was studied. Pearson's correlation and Spearman's rho was used for correlating cell size parameters with potential influencing variables. All the statistical analysis was performed with MINITAB 18.1 software.

Nomenclature

a	spread of size distribution (dimensionless)
C	coil counts (dimensionless)
C_{LOUT}	outlet liquid CO_2 concentration (mmol l^{-1})
D	dilution rate (h^{-1})
F_{CO_2}	inlet CO_2 gas flow (l h^{-1})
F_{in}	bioreactor inlet gas flow (l h^{-1})
F_{out}	bioreactor total outlet gas flow (l h^{-1})
HRT	hydraulic residence time (days)
L	trichome length (μm)
O_{2out}	outlet O_2 fraction (%)
P	pitch size (μm)
PAR	photosynthetically active radiation. It comprises light between 400 and 700 nm
PFD	photon flux density (μmol m^{-2} s^{-1})
PPFD	photosynthetic photon flux density (μmol m^{-2} s^{-1}). Referred to the PAR region (400–700 nm)
PQ	photosynthetic quotient ($mol_{O2} \cdot mol_{CO2}{}^{-1}$)
q_{O_2}	specific O_2 production (mmol l^{-1} h^{-1})
q_{CO_2}	specific CO_2 consumption (mmol l^{-1} h^{-1})
qPFD	specific photon flux density per unit of biomass (μmol g^{-1} s^{-1})
r	regression coefficient (dimensionless)
r_{CO_2}	CO_2 volumetric consumption rate (mmol l^{-1} h^{-1})
r_{O_2}	O_2 volumetric production rate (mmol l^{-1} h^{-1})
r_X	biomass volumetric production rate (g l^{-1} h^{-1})
S	cumulative cell parameter distribution (dimensionless)
t	time (days)
V_R	bioreactor volume (l)
W	trichome width (μm)
X	biomass concentration (g l^{-1})
x	size parameter (μm)
k	half-saturation constant for a given size parameter (μm)
X_{COUT}	molar fraction of CO_2 in the outlet gas (mol mol^{-1})
X_{CIN}	molar fraction of CO_2 in the inlet gas (mol mol^{-1})

Greek letters

γ	bioreactor volume illuminated fraction (dimensionless)

Acknowledgements

MELiSSA is an international consortium of 15 partners led by the European Space Agency (for information: https://www.melissafoundation.org). Its activities are governed by a Memorandum of Understanding (ESA 4000100293/10/NL/PA). The MELiSSA Pilot Plant is funded from ESA contributions from Spain (main contributor), Begium, France, Italy and Norway, under Frame Contract C4000109802/13/NL/CP. Co-funding from Ministerio de Ciencia e Innovación (RD 788/2020), Generalitat de Catalunya and Universitat Autònoma de Barcelona is also acknowledged.

Conflict of interest

None declared.

References

Ahmed, M., Moerdijk-Poortvliet, T.C.W., Wijnholds, A., Stal, L.J., and Hasnain, S. (2014) Isolation, characterization and localization of extracellular polymeric substances from the cyanobacterium *Arthrospira platensis* strain MMG-9. *Eur J Phycol* **49:** 143–160.

Alemany, L., Peiro, E., Arnau, C., Garcia, D., Poughon, L., Cornet, J.-F., *et al*. (2019) Continuous controlled long-term operation and modeling of a closed loop connecting an air-lift photobioreactor and an animal compartment for the development of a life support system. *Biochem Eng J* **151:** 107323.

Allakhverdiev, S.I., Tsvetkova, N., Mohanty, P., Szalontai, B., Byoung, Y.M., Debreczeny, M., and Murata, N. (2005) Irreversible photoinhibition of photosystem II is caused by exposure of Synechocystis cells to strong light for a prolonged period. *Biochim Biophys Acta - Bioenerget* **1708:** 342–351.

Barbosa, M.J., Janssen, M., Ham, N., Tramper, J., and Wijffels, R.H. (2003) Microalgae cultivation in air-lift reactors: modeling biomass yield and growth rate as a function of mixing frequency. *Biotechnol Bioeng* **82:** 170–179.

Begum, H., Yusoff, F.M.D., Banerjee, S., Khatoon, H., and Shariff, M. (2016) Availability and utilization of pigments from microalgae. *Crit Rev Food Sci Nutr* **56:** 2209–2222.

Bennett, A., and Bogorad, L. (1973) Complementary chromatic adaptation in a filamentous blue-green alga. *J Cell Biol* **58:** 419–435.

Bhattacharya, S., and Shivaprakash, M.K. (2005) Evaluation of three Spirulina species grown under similar conditions for their growth and biochemicals. *J Sci Food Agric* **85:** 333–336.

Chakdar, H., and Pabbi, S. (2015) Cyanobacterial phycobilins: production, purification, and regulation. In *Frontier Discoveries and Innovations in Interdisciplinary Microbiology*. New Delhi: Springer, pp.45–69.

Charon, J., Blanco, S., Cornet, J.-F., Dauchet, J., El Hafi, M., Fournier, R., *et al*. (2016) Monte Carlo implementation of Schiff's approximation for estimating radiative properties of homogeneous, simple-shaped and optically soft particles: application to photosynthetic micro-organisms. *J Quant Spectrosc Radiat Transfer* **172:** 3–23.

Chen, H.-B., Wu, J.-Y., Wang, C.-F., Fu, C.-C., Shieh, C.-J., Chen, C.-I., *et al*. (2010) Modeling on chlorophyll a and phycocyanin production by *Spirulina platensis* under various light-emitting diodes. *Biochem Eng J* **53:** 52–56.

Cheng, J., Guo, W., Ameer Ali, K., Ye, Q., Jin, G., and Qiao, Z. (2018) Promoting helix pitch and trichome length to improve biomass harvesting efficiency and carbon dioxide fixation rate by Spirulina sp. in 660 m2 raceway ponds under purified carbon dioxide from a coal chemical flue gas. *Biores Technol* **261:** 76–85.

Ciferri, O. (1983) Spirulina, the edible microorganism. *Microbiol Rev* **47:** 551–578.

Clauwaert, P., Muys, M., Alloul, A., De Paepe, J., Luther, A., Sun, X., *et al*. (2017) Nitrogen cycling in Bioregenerative Life Support Systems: challenges for waste refinery and food production processes. *Prog Aerosp Sci* **91:** 87–98.

Cogne, G., Gros, J.B., and Dussap, C.G. (2003a) Identification of a Metabolic Network Structure Representative of Arthrospira (Spirulina) platensis Metabolism. *Biotechnol Bioeng* **84:** 667–676.

Cogne, G., Lehmann, B., Dussap, C.G., and Gros, J.B. (2003b) Uptake of macrominerals and trace elements by the cyanobacterium *Spirulina platensis* (Arthrospira platensis PCC 8005) under photoautotrophic conditions: culture medium optimization. *Biotechnol Bioeng* **81:** 588–593.

Cornet, J.F. (2007) *Procédés Limités par le Transfert de Rayonnement en Milieu Hétérogène Étude des Couplages Cinétiques et Énergétiques dans les Photobioréacteurs par une Approche*. Thermodynamique. Sciences de l'ingénieur [physics]. URL https://hal.archives-ouvertes.fr/tel-01281239

Cornet, J.F., Dussap, C.G., and Gros, J.B. (1998) Kinetics and energetics of photosynthetic micro-organisms in photobioreactors. *Bioprocess Algae Reactor Technol Apoptosis* **59:** 153–224.

Dauchet, J., Blanco, S., Cornet, J.F., and Fournier, R. (2015) Calculation of the radiative properties of photosynthetic microorganisms. *J Quant Spectrosc Radiat Transfer* **161:** 60–84.

Dauchet, J., Cornet, J.F., Gros, F., Roudet, M., and Dussap, C.G. (2016) Photobioreactor modeling and radiative transfer analysis for engineering purposes. In *Advances in Chemical Engineering*, Vol. **48.** Legrand, J. (ed.). Burlington: Academic Press, pp. 1–106.

De Lorimier, R.M., Smith, R.L., and Stevens, S.E. (1992) Regulation of phycobilisome structure and gene expression by light intensity. *Plant Physiol* **98:** 1003–1010.

De Oliveira, M.A.C.L., Monteiro, M.P.C., Robbs, P.G., and Leite, S.G.F. (1999) Growth and chemical composition of Spirulina maxima and Spirulina platensis biomass at different temperatures. *Aquac Int* **7:** 261–275.

Depraetere, O., Pierre, G., Deschoenmaeker, F., Badri, H., Foubert, I., Leys, N., *et al*. (2015) Harvesting carbohydrate-rich Arthrospira platensis by spontaneous settling. *Biores Technol* **180:** 16–21.

Follstad, B.D., Balcarcel, R.R., Stephanopoulos, G., and Wang, D.I.C. (1999) Metabolic flux analysis of hybridoma continuous culture steady state multiplicity. *Biotechnol Bioeng* **63:** 675–683.

Gòdia, F., Albiol, J., Pérez, J., Creus, N., Cabello, F., Montràs, A., *et al*. (2004) The MELISSA pilot plant facility as an integration test-bed for advanced life support systems. *Adv Space Res* **34:** 1483–1493.

Gupta, P.L., Lee, S.M., and Choi, H.J. (2015) A mini review: photobioreactors for large scale algal cultivation. *World J Microbiol Biotechnol* **31:** 1409–1417.

Hendrickx, L., De Wever, H., Hermans, V., Mastroleo, F., Morin, N., Wilmotte, A., *et al*. (2006) Microbial ecology of the closed artificial ecosystem MELiSSA (Micro-Ecological Life Support System Alternative): Reinventing and compartmentalizing the Earth's food and oxygen regeneration system for long-haul space exploration missions. *Res Microbiol* **157:** 77–86.

Herbert, D., Phipps, P.J., and Strange, R.E. (1971) Chemical analysis of microbial cells. *Methods Microbiol* **5:** 209–344.

Hihara, Y., Kamei, A., Kanehisa, M., Kaplan, A., and Ikeuchi, M. (2001) DNA microarray analysis of cyanobacterial gene expression during acclimation to high light. *Plant Cell* **13:** 793–806.

Jensen, S., and Knutsen, G. (1993) Influence of light and temperature on photoinhibition of photosynthesis in Spirulina platensis. *J Appl Phycol* **5:** 495–504.

Kaggwa, M.N., Burian, A., Oduor, S.O., and Schagerl, M. (2013) Ecomorphological variability of Arthrospira

fusiformis (Cyanoprokaryota) in African soda lakes. *MicrobiologyOpen* **2:** 881–891.
Kiss, B., and Németh, Á. (2016) Application of a high cell density capacitance sensor to different microorganisms. *Periodica Polytech Chem Eng* **60:** 290–297.
Lasseur, C., Brunet, J., Weever, H.D., Dixon, M., Dussap, G., Godia, F., *et al.* (2010) MELiSSA: The European project of closed life support system. *Gravity Space Biol* **23:** 3–12.
Ma, Z., and Gao, K. (2010) Spiral breakage and photoinhibition of Arthrospira platensis (Cyanophyta) caused by accumulation of reactive oxygen species under solar radiation. *Environ Exp Bot* **68:** 208–213.
Markou, G., Chatzipavlidis, I., and Georgakakis, D. (2012) Effects of phosphorus concentration and light intensity on the biomass composition of Arthrospira (Spirulina) platensis. *World J Microbiol Biotechnol* **28:** 2661–2670.
Masot, A. (2007) *Engineering Photosynthetic Systems for Bioregenerative Life Support*. Bellatera, Spain: Universitat Autonòma de Barcelona.
Mattoo, A.K., Marder, J.B., and Edelman, M. (1989) Dynamics of the photosystem II reaction center. *Cell* **56:** 241–246.
Mergeay, M., Verstraete, W., Dubertret, G., Lefort-tran, M., Chipaux, C., and Binot, R. (1988) MELiSSA. A Microorganisms Based Model for CELSS Development. In *Proc. 3rd Symp. Sp. Therm. Control Life Support Syst*. Noordwijk, The Netherlands, pp. 65–68.
Miron, A.S., Camacho, F.G., Gómez, A.C., Grima, E.M., and Chisti, Y. (2000) Bubble-column and airlift photobioreactors for algal culture. *AIChE J* **46:** 1872–1887.
Mühling, M., Harris, N., Belay, A., and Whitton, B.A. (2003) Reversal of helix orientation in the cyanobacterium Arthrospira. *J Phycol* **39:** 360–367.
Mulukutla, B.C., Yongky, A., Grimm, S., Daoutidis, P., and Hu, W.S. (2015) Multiplicity of steady states in glycolysis and shift of metabolic state in cultured mammalian cells. *PLoS One* **10:** 1–20.
Muramatsu, M., and Hihara, Y. (2012) Acclimation to high-light conditions in cyanobacteria: from gene expression to physiological responses. *J Plant Res* **125:** 11–39.
Nomsawai, P., Tandeau De Marsac, N., Thomas, J.C., Tanticharoen, M., and Cheevadhanarak, S. (1999) Light regulation of phycobilisome structure and gene expression in Spirulina platensis C1 (Arthrospira sp. PCC 9438). *Plant Cell Physiol* **40:** 1194–1202.
Ogato, T., and Kifle, D. (2014) Morphological variability of Arthrospira (Spirulina) fusiformis (Cyanophyta) in relation to environmental variables in the tropical soda lake Chitu, Ethiopia. *Hydrobiologia* **738:** 21–33.
Patel, A., Mishra, S., Pawar, R., and Ghosh, P.K. (2005) Purification and characterization of C-Phycocyanin from cyanobacterial species of marine and freshwater habitat. *Protein Expr Purif* **40:** 248–255.
Pilon, L., Berberoğlu, H., and Kandilian, R. (2011) Radiation transfer in photobiological carbon dioxide fixation and fuel production by microalgae. *J Quant Spectrosc Radiat Transfer* **112:** 2639–2660.
Porra, R.J. (2002) The chequered history of the development and use of simultaneous equations for the accurate determination of chlorophylls a and b. *Photosynth Res* **73:** 149–156.
Poughon, L., Farges, B., Dussap, C.G., Godia, F., and Lasseur, C. (2009) Simulation of the MELiSSA closed loop system as a tool to define its integration strategy. *Adv Space Res* **44:** 1392–1403.
Richmond, A., Lichtenberg, E., Stahl, B., and Vonshak, A. (1990) Quantitative assessment of the major limitations on productivity of Spirulina platensis in open raceways. *J Appl Phycol* **2:** 195–206.
Rodríguez, H., Rivas, J., Guerrero, M.G., and Losada, M. (1991) Enhancement of phycobiliprotein production in nitrogen-fixing cyanobacteria. *J Biotechnol* **20:** 263–270.
Silva, J.P., Almeida, Y.B., Pinheiro, I.O., Knoelchelmann, A., and Silva, J.M.F. (2015) Multiplicity of steady states in a bioreactor during the production of 1,3-propanediol by Clostridium butyricum. *Bioprocess Biosyst Eng* **38:** 229–235.
Tomaselli, L., Boldrini, G., and Margheri, M.C. (1997) Physiological behaviour of Arthrospira (Spirulina) maxima during acclimation to changes in irradiance. *J Appl Phycol* **9:** 37–43.
Vernerey, A., Albiol, J., Lasseur, C., and Godia, F. (2001) Scale-up and design of a pilot-plant photobioreactor for the continuous culture of *Spirulina platensis*. *Biotechnol Prog* **17:** 431–438.
Vonshak, A. (2002) *Spirulina platensis* (Arthrospira): Physiology, Cell-biology and Biotechnology. London: Taylor & Francis.
Vonshak, A., Chanawongse, L., Bunnag, B., and Tanticharoen, M. (1996) Light acclimation and photoinhibition in three *Spirulina platensis* (cyanobacteria) isolates. *J Appl Phycol* **8:** 35–40.
Vonshak, A., Cheung, S.M., and Chen, F. (2000) Mixotrophic growth modifies the response of Spirulina (Arthrospira) platensis (Cyanobacteria) cells to light. *J Phycol* **36:** 675–679.
Vonshak, A., Guy, R., Poplawsky, R., and Ohad, I. (1988) Photoinhibition and its recovery in two strains of the cyanobacterium spirulina platensis. *Plant Cell Physiol* **29:** 721–726.
Zhang, W. & Song, X. (2018) Synthetic biology of Cyanobacteria. In *Advances in Experimental Medicine and Biology*. Singapore: Springer, pp.75–96.
Wellburn, A.R. (1994) The spectral determination of Chlorophylls a and b, as well as total carotenoids, using various solvents with spectrophotometers of different resolution. *J Plant Physiol* **144:** 307–313.
Wu, H., Gao, K., Villafañe, V.E., Watanabe, T., and Helbling, E.W. (2005) Effects of solar UV radiation on morphology and photosynthesis of filamentous cyanobacterium Arthrospira platensis. *Appl Environ Microbiol* **71:** 5004–5013.
Yongky, A., Lee, J., Le, T., Mulukutla, B.C., Daoutidis, P., and Hu, W.S. (2015) Mechanism for multiplicity of steady states with distinct cell concentration in continuous culture of mammalian cells. *Biotechnol Bioeng* **112:** 1437–1445.

Supporting information

Additional supporting information may be found online in the Supporting Information section at the end of the article.

Supporting Information